Available online at www.sciencedirect.com
SCIENCE DIRECT®
Tectonophysics 377 (2003) 197–209
TECTONOPHYSICS
www.elsevier.com/locate/tecto

Record of deformation by secondary magnetic remanences and magnetic anisotropy in the Nar/Phu valley (central Himalaya)

E. Schill[a,b,*], E. Appel[a], L. Godin[c,1], C. Crouzet[a], P. Gautam[a,d], K.R. Regmi[d]

[a] *Institut für Geologie, Universität Tübingen, Sigwartstraße 10, 72076, Tüubingen Germany*
[b] *Institut für Geophysik, ETH Zürich, Hönggerberg HPP O14, 8093 Zurich, Switzerland*
[c] *Department of Earth Sciences, Simon Fraser University, Burnaby, Canada, V5A1S6*
[d] *Central Department of Geology, Tribhuvan University, Kirtipur, Kathmandu, Nepal*

Received 3 October 2002; received in revised form 6 June 2003; accepted 25 August 2003

Abstract

Secondary magnetic remanences residing in pyrrhotite and anisotropy of magnetic susceptibility (AMS) were studied in low-grade metamorphic carbonates of the Tethyan Himalaya in Nar/Phu valley (central Nepal) and used for interpretation of tectonic deformations. The characteristic remanence (ChRM) is likely of thermomagnetic origin related to post-peak metamorphic cooling occurring after the Eohimalayan phase (35–32 Ma). The ChRM postdates small-scale folding (main Himalayan folding F1 and F2) as shown by a negative fold test of site mean directions at 99% confidence level, and has been probably acquired between 32 and 25 Ma. Late-orogenic long-wavelength folding associated with the Chako antiform (CA) is recorded by the spatial dispersion of ChRM directions and the distribution of the main axes of the AMS tensor. The mean tilting of the ChRM direction since remanence acquisition (≈ 20–30°) approximately coincides with the tilting of the CA (31°) at the study area indicating that the pyrrhotite remanence predates the CA (CA formed at < 18 Ma according to preliminary U/Pb dating). However, comparison of tilt angles of remanence directions and AMS tensor axes suggests that remanence acquisition was not completed before the onset of the CA formation. This could imply a younger age (Early Miocene or even younger) of the ChRM. Using the distribution of remanence directions along a small-circle as well as the distribution of AMS tensor axes, a clockwise mean rotation of 16° is obtained for a remanence age of ≈ 30 Ma. An Early Miocene remanence age would not change this result substantially. Compilation of rotations in the Tethyan Himalaya deduced from secondary pyrrhotite remanences reveals an increasing clockwise rotation from the Hidden valley in the W to the Shiar valley in the E (≈ 150 km distance), incompatible with an oroclinal bending model.

Keywords: Palaeomagnetism; Himalaya; Rotation; Secondary magnetization; Magnetic anisotropy; Pyrrhotite

1. Introduction

The India–Asia collision and ongoing convergence between the two continents resulted in an intensively deformed continental margin of India, building up the Himalayan orogen. Several deformation phases characterize the tectono-metamorphic

* Corresponding author. Institut für Geophysik, ETH Zürich, Hönggerberg HPP O14, 8093 Zurich, Switzerland. Tel.: +41-01-6333667; fax: +41-01-6331065.
E-mail address: schill@mag.ig.erdw.ethz.ch (E. Schill).
[1] Now at: Department of Geological Sciences and Geological Engineering, Miller Hall, Queen's University, Kingston, Ontario, Canada K7L 3N6.

0040-1951/$ - see front matter © 2003 Elsevier B.V. All rights reserved.
doi:10.1016/j.tecto.2003.08.020

evolution of the Himalayan Arc and account for significant continental shortening. One or two metamorphic events caused almost complete overprint of magnetic remanences throughout most areas. However, it has been shown in several mountain belts, that secondary remanence directions provide meaningful information on the tectonic evolution of orogens (e.g. Klootwijk et al., 1985; Appel et al., 1991; Thomas et al., 1999; Enkin et al., 2000). Rotation angles and tectonic tilting since the time of remanence acquisition can be extracted from secondary synfolding remanence directions using the small-circle reconstruction method of Waldhör et al. (2001). The idea of the small-circle distribution and back-tilting of the observed remanence direction to the one expected from the apparent polar wander path (APWP) has been successfully applied to reconstruct the amount of rotational shortening on the Indian margin for a one-stage tilting (Schill et al., 2001). In the western Himalaya, only a single phase of long-wavelength folding (approximately >10 km wavelength) is identified by structural (Wyss et al., 1999) as well as palaeomagnetic (Schill et al., 2001, in press) observations. In contrast, in the Nar/Phu valley of central Nepal, structural analyses indicate a two-stage folding/tilting of larger wavelength of approximately >5 km (Godin, 2001). New palaeomagnetic results from the Nar/Phu valley (north of the Annapurna range in the Tethyan Himalaya, 28.8°N, 84.3°E; Fig. 1) show the relation between the calculated tilting and structural features of the area. An integrated approach using magnetic anisotropy, secondary remanences, structural geology, and radiometric dating lead to resolution of different stages in the late-orogenic deformation history of the area.

2. Structural geology and age constraints

The stratigraphic sequence in the Nar/Phu valley is demarcated to the S by the South Tibetan detachment system (Searle and Godin, in press) and comprises Silurian/Devonian carbonates to the Jurassic Kioto Limestone (Fuchs et al., 1999, Fig. 2a). The Scythian–Anisian Tamba Kurkur Formation is missing. The tectono-metamorphic evolution of the Nar/Phu valley is characterised by several deformation phases and related metamorphic events (Table 1). Generally, the oldest deformation phase (south-verging Himalayan folding; F1) is assumed to be of short-wavelength character and attributed to a pre-Eohimalayan (Godin et al., 2001) or Eohimalayan event (DeCelles et al., 1998; Hodges et al., 1996; Vannay and Hodges, 1996). It is generally accepted that Eohimalayan metamorphism in the High Himalayan Crystalline (HHC) of Nepal occurred at about 35–30 Ma (Godin et al., 1999; Godin et al., 2001; Vannay and Hodges, 1996; Coleman and Hodges, 1998). In the Nar/Phu valley, the late Palaeozoic/Mesozoic sediments are folded in north-verging direction (F2) and just S of Phu village later truncated by the Pangla Ri fault (Godin, 2001; Fig. 2b). This fault marks the boundary between the low-grade Palaeozoic/Mesozoic metamorphic sequence and the high-grade metamorphic older sediments with predominantly south-verging deformation (Godin, 2001). In Thakkhola area, the north-verging megascopic folds have been attributed to an age of about 35 Ma (Godin et al., 1999, 2001) using kyanite grade-melt in the upper part of the HHC. This is consistent with a peak temperature postdating the deformation, estimated at 30–25 Ma by Crouzet et al. (2002) using illite K/Ar and zircon fission track datings in the Manang area. The folding of the Chako antiform caused a major tilting to the N in the sampling area. Three possible explanations for the dome shape are: (1) the relation of the dome to late folding and doming of the HHC (Le Fort and Guillot, 1998; Godin, 2001), (2) late granitic intrusion and diapiric doming (Godin, 2001) and (3) doming as a result of isostatic re-adjustment following crustal extension (Godin, 2001). Preliminary zircon concordant U–Pb ages from a folded and boudinaged dyke in the Chako antiform provide an age of 18 Ma. The structural constraints indicate a maximum age for the fold-related deformation of 18 Ma.

The sampling area is located in the area around Phu village (Fig. 2a). In total, 14 palaeomagnetic sites were taken from the Permian limestones (2 sites), Triassic Mukut limestones (9 sites), and Carboniferous limestones (3 sites). The general mineralogy of such carbonates are described from microscopic observations. The carbonates are usually

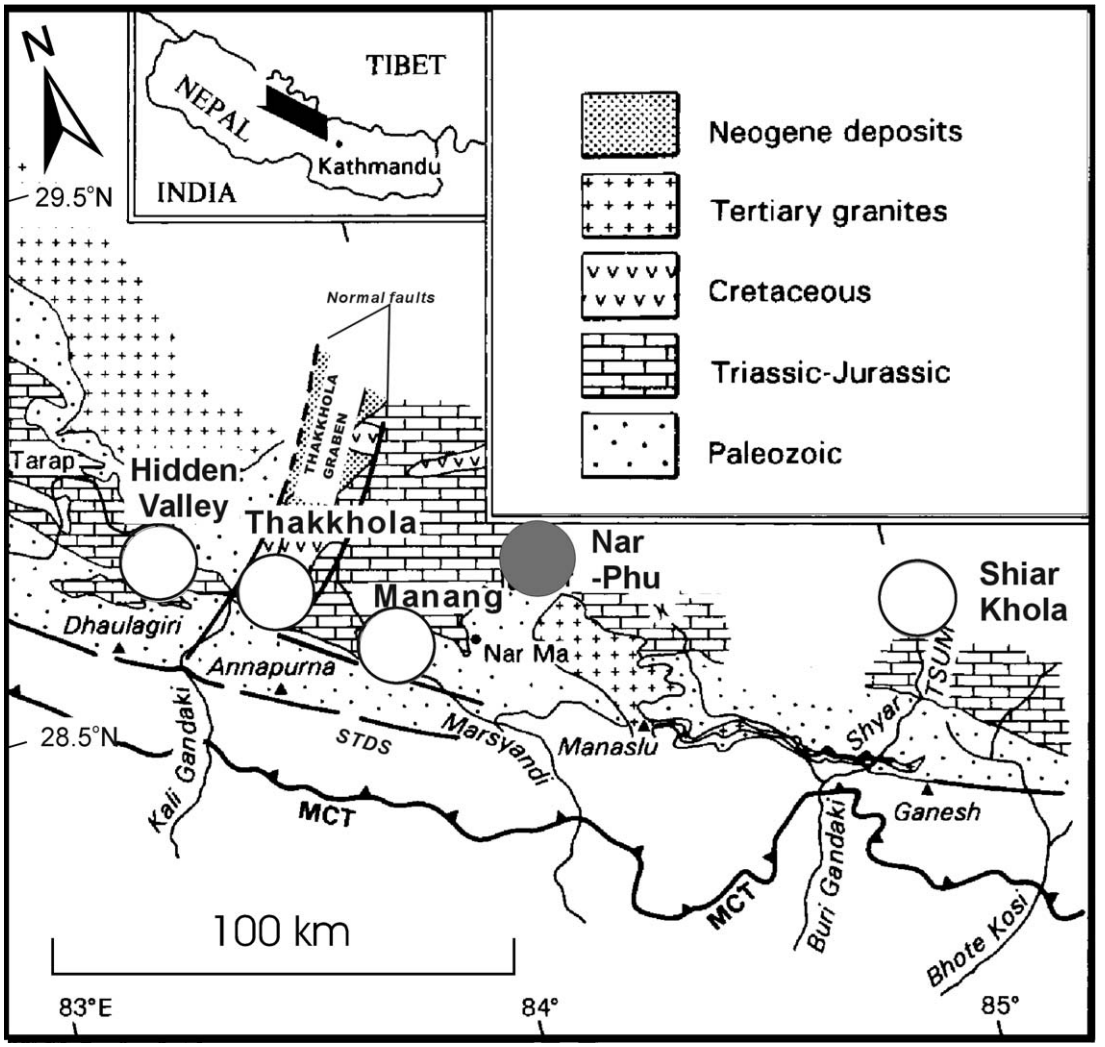

Fig. 1. Geological sketch map of the Tethyan Himalaya in central Nepal (after Garzanti, 1999) showing the study area (grey circle) and neighbouring areas from where data are already published (open circles). MCT: Main Central Thrust; STDS: South Tibetan Detachment System.

siliceous limestones, with micritic and sometimes-sparry calcite ranging from 80% to 90% with quartz clasts (10% to 15%) and about 5% opaque minerals (ilmenite clasts, leucoxene, sulphides and organic matter). Some samples contain minor amount of detrital mica (< 1%). Sparry calcite is more abundant in samples from the lower part of the sedimentary sequence. According to Le Fort and Guillot (1998), the sampling is a typical example for interference of north- and south-verging tectonics. South-verging kink folds (F4) as defined in the adjacent Thakkhola area (Godin et al., 1999; Godin, in press) also occur in the Phu area. South of the sampling area, the so-called Chako antiform dominates the structural geometry in the Nar/Phu valley.

3. Sample treatment and analytical procedure

In general, about 10 cores, 2.5 cm in diameter, were taken and cut into specimens of standard size (2.2 cm length). All magnetic measurements were

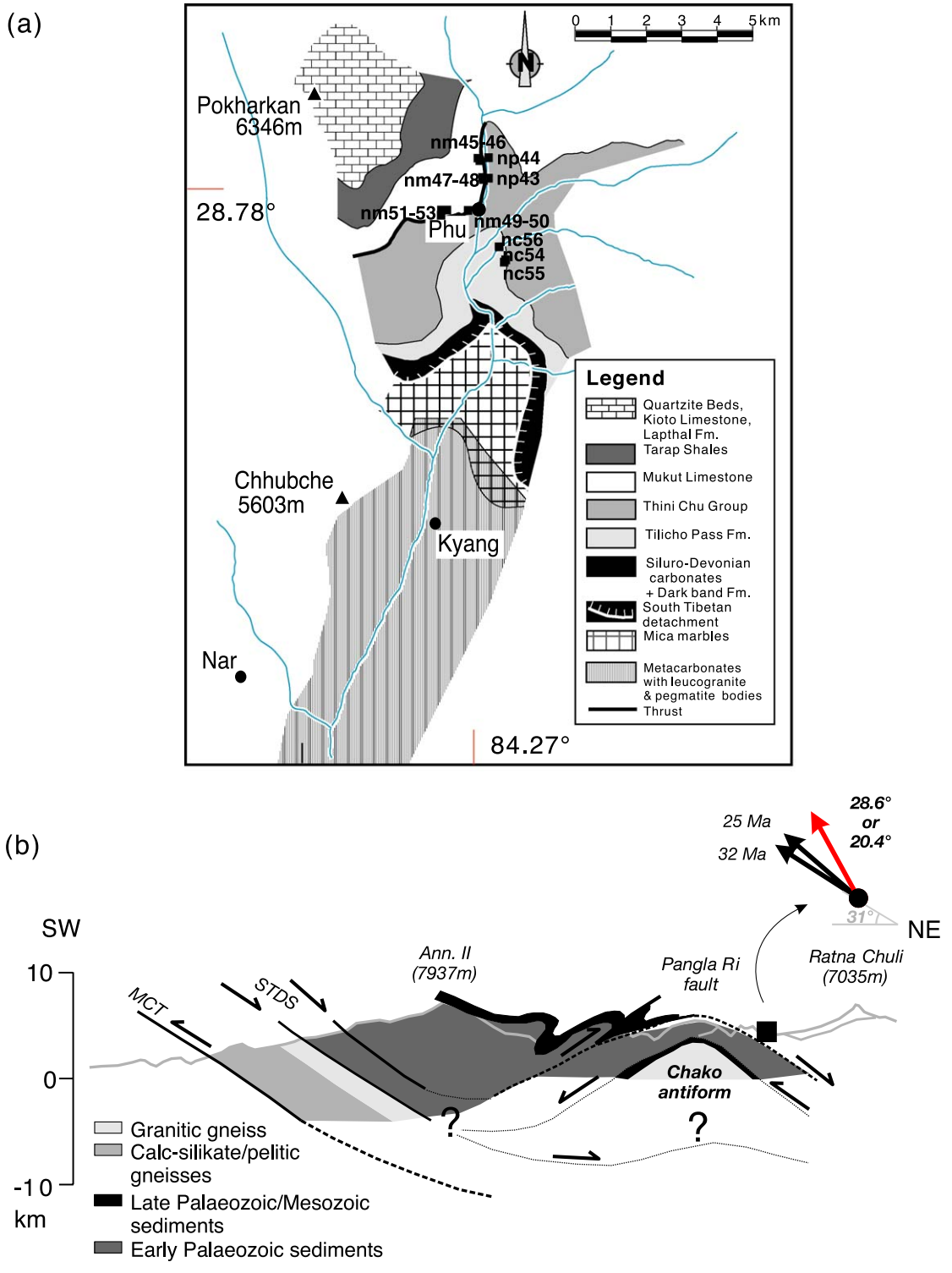
(a)
0 1 2 3 4 5km
N
Pokharkan
6346m
nm45-46
np44
nm47-48
np43
28.78°
nm51-53
Phu
nm49-50
nc56
nc54
nc55
Chhubche
5603m
Kyang
Nar
84.27°
Legend
Quartzite Beds, Kioto Limestone, Lapthal Fm.
Tarap Shales
Mukut Limestone
Thini Chu Group
Tilicho Pass Fm.
Siluro-Devonian carbonates + Dark band Fm.
South Tibetan detachment
Mica marbles
Metacarbonates with leucogranite & pegmatite bodies
Thrust
(b)
25 Ma
32 Ma
28.6° or 20.4°
31°
NE
SW
10
0
-10
km
MCT
STDS
Ann. II
(7937m)
Pangla Ri
fault
Ratna Chuli
(7035m)
Chako
antiform
?
?
Granitic gneiss
Calc-silikate/pelitic gneisses
Late Palaeozoic/Mesozoic sediments
Early Palaeozoic sediments

Table 1
Summary of structural events observed in the Tethyan Himalaya of the Nar/Phu area (central Nepal) and their respective ages

Phase	Timing[a]		Structural features[b,c]
	ca. 14 Ma		SW NE
D_4		- Renewed southwest-verging shortening - South-verging kink folds and crenulation cleavage - Large amplitude folds (i.e., Chako antiform)	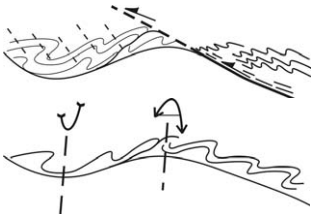
	ca. 18 Ma		
D_3	ca .22 Ma	- Top-to-the-north normal faults (i.e., Pangla Ri fault), related to the South Tibetan detachment system	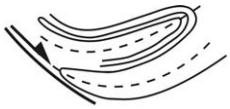
D_2	ca.35 Ma	- Northeast-verging megascopic folds (long wavelength)	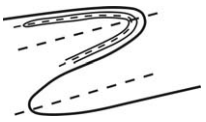
D_1	ca. 45 Ma	- Early south-verging nappe structures - locally preserved rootless isoclinal folds (short wavelength)	

[a]Godin et al. (2001).
[b]Godin (2003).
[c]Searle and Godin (2003).

carried out in the palaeomagnetic laboratory at the University of Tübingen (Germany). For two pilot samples from each site, the natural remanent magnetization (NRM) was progressively demagnetized, one by heating in a furnace MMTD1 (Magnetic Measurements) and the other by alternating fields (AF) using a 2G600 automatic degaussing system (2G Enterprises). Remanence directions were measured with a SQUID magnetometer 755R from 2G Enterprises (noise level <0.01 mA m^{-1} for 10 cm^3 specimens). Low-field magnetic susceptibility was monitored after each heating step to detect possible changes in magnetic mineralogy. The AF-demagnetized specimens were then subjected to isothermal remanence (IRM) acquisition by using a pulse magnetizer MMPM9 (Magnetic Measurements) with a maximum field of 2.5 T and subsequent stepwise thermal demagnetization of the saturation IRM (SIRM). The remaining specimens were thermally demagnetized in 5–50 °C steps. Anisotropy of magnetic susceptibility was measured with a KLY-2 susceptibility bridge (Agico); tensor statistics and parameter determination after Jelinek (1978) were applied.

Fig. 2. (a) Geological map of the Phu area (modified after Fuchs et al., 1999) with sampling sites (full squares). (b) Structural profile across the Main Himalayan features in the Nar/Phu valley and adjacent areas (Godin, 2001). The black arrows represent the expected remanence inclination from the APWP (Acton, 1999) for an acquisition age ranging from 32 to 25 Ma. The grey arrow represents the observed overall remanence inclination for the sampling area, resulting in a northward tilting of 28.6° and 20.4°, respectively. The 31°-angle denotes the slope of the Chako antiform at the sampling area.

4. Anisotropy of low-field magnetic susceptibility (AMS)

Principle axes of the AMS tensor (maximum: k1, intermediate: k2, minimum: k3), bulk susceptibility and factors for the anisotropy degree (P') and shape (T) are listed in Table 2 for site means. All results mentioned below are in geographic co-ordinates.

In Permo-Triassic sites, two major patterns (P1 and P2) of the AMS tensor axes distribution are observed. Both patterns are coexisting in most of the sites, i.e. different specimens from a single site are dominated by the characteristics of either P1 or P2. It can be assumed that P1 and P2 are controlled by different (para- or ferri-)magnetic mineral components, and variation of their contents decides which pattern is identified.

P1 is characterised by well-grouped k3 axes for single specimens (Fig. 3a) and site means (Fig. 3c), aligned approximately parallel to the fold axis. Directions of k1 and k2 axes are randomly oriented even for specimens within single sites. Bulk susceptibility of P1 is generally low (site means 15–158e − 6 SI) and the degree of anisotropy ranges is between 1.01 and 1.04; a slight dominance of oblate shape is indicated (Fig. 3d and Table 2).

P2 is found in samples with relatively higher bulk susceptibility (12–676e − 6 SI) and a higher degree of anisotropy (1.03 to 1.19). The shape is generally prolate (Fig. 3d and Table 2) with well-grouped k1 axes for specimens within sites (Fig. 3b) as well as for site means (Fig. 3c). For P2, the k1 directions coincide with the fold axis (Fig. 3c). Within sites, also k2 and k3 are well grouped (except nm53), whereas they are somewhat more scattered at site mean level (Fig. 3c).

The Carboniferous sites show a strong degree of anisotropy, and a different distribution of tensor axes.

Table 2
Statistical parameters for AMS patterns P1 and P2 using tensor statistics after Jelinek (1978)

Site	Sus (10e − 6 SI)	k1	k2	k3	k1	k2	k3	*N*	P′	*T*
		(Geographic co-ordinates)			(Stratigraphic co-ordinates)					
Pattern 1										
np43	–	–	–	–	–	–	–	–	–	–
np44	106	198/19	53/67	292/12	202/64	31/26	298/4	9	1.01	0.17
nm45	28	17/21	16/65	282/14	197/24	18/20	295/16	7	1.02	0.08
nm46	59	44/45	205/43	304/10	36/8	235/82	127/2	7	1.03	0.15
nm47	121	200/48	1/41	99/10	18/37	201/52	110/2	8	1.04	0.31
nm48	15	340/26	220/46	89/33	164/7	281/75	73/14	3	1.03	− 0.36
nm49	60	132/71	26/5	294/18	195/17	4/73	104/4	12	1.04	0.22
nm50	24	102/72	357/5	266/17	182/64	351/26	84/5	5	1.04	0.04
nm51	158	188/39	44/45	294/19	200/29	27/61	292/3	10	1.03	0.03
nm52	130	37/9	137/50	300/39	22/41	194/50	288/4	10	1.02	− 0.13
nm53	112	184/32	46/50	288/21	201/25	2/64	107/8	6	1.02	− 0.01
Pattern 2										
np43	676	106/29	197/1	288/61	268/1	177/66	359/25	12	1.07	− 0.45
np44	–	–	–	–	–	–	–	–	–	–
nm45	199	113/2	204/14	16/75	111/4	208/59	19/30	5	1.07	− 0.42
nm46	162	119/5	28/7	244/81	113/11	210/32	7/56	4	1.05	− 0.58
nm47	538	94/11	274/79	184/0	111/7	201/3	314/83	3	1.19	0.17
nm48	24	208/38	318/24	72/42	231/76	326/2	57/13	7	1.03	− 0.08
nm49	–	–	–	–	–	–	–	–	–	–
nm50	12	125/36	224/12	330/51	146/33	44/18	291/51	3	1.07	− 0.40
nm51	–	–	–	–	–	–	–	–	–	–
nm52	–	–	–	–	–	–	–	–	–	–
nm53	376	300/19	210/0	120/71	189/7	27/15	235/74	6	1.10	− 0.23

Sus: susceptibility; k1, k2, k3: declination/inclination of maximum, intermediate, minimum axes of the anisotropy tensor. *N*: number of specimens. Degree of anisotropy $P' = \exp[(2((\ln(k1) - n)2 + (\ln(k2) - n)2 + (\ln(k3) - n)2)1/2]$ with $n = 1/3(\ln(k1) + \ln(k2) + \ln(k3))$; shape factor $T = (\ln F - \ln L)/(\ln F + \ln L)$ with $F = k2/k3$, $L = k1/k2$.

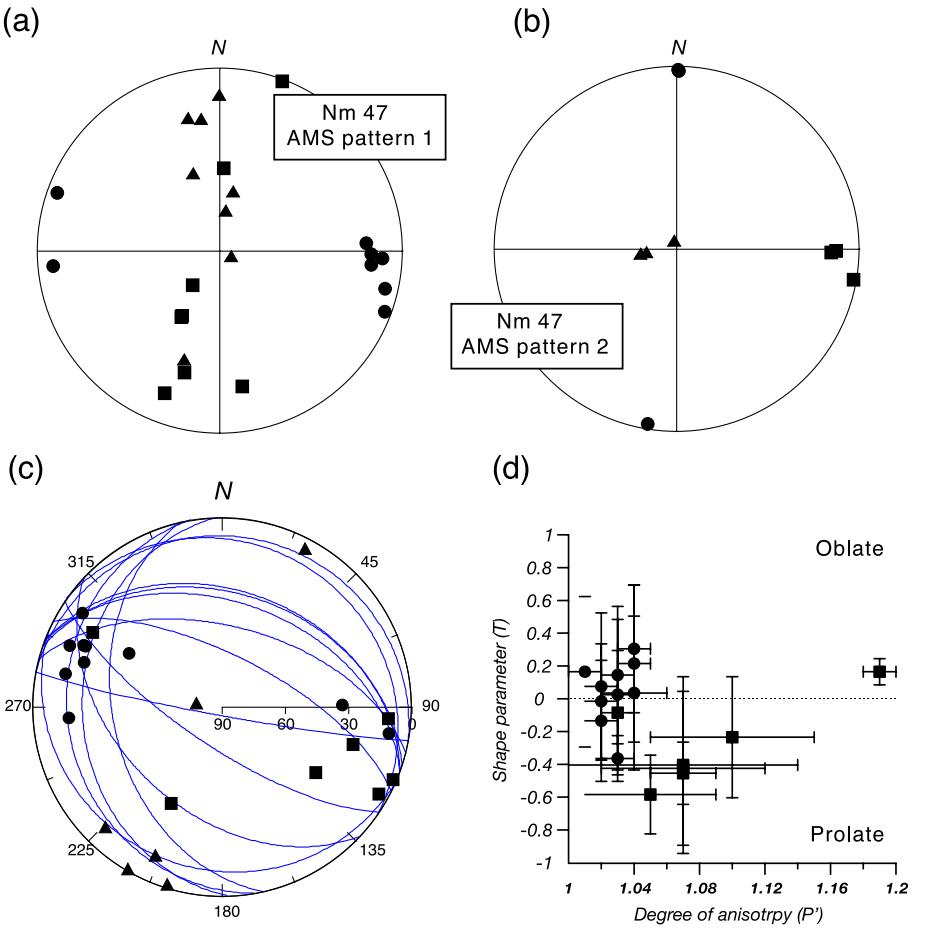

Fig. 3. Single specimen directions of the main axes of the anisotropy tensor with k1 (maximum, squares), k2 (intermediate, triangles) and k3 (minimum susceptibility, circles) for site nm47, representing AMS pattern P1 (a) and P2 (b). (c) Site mean directions of AMS patterns P1 (k3: circles) and P2 (k1: squares, k2: triangles) as well as bedding planes (great circles), showing the consistency between fold axis (intersection of bedding planes), k3 of P1 and k1 of P2. (d) Degree of anisotropy (P') versus shape factor (T) of AMS from the Permo-Triassic metasediments. Circles/squares: P1/P2.

However, because of the low number of sites ($n=3$) they are not further considered for interpretation.

5. Magneto-mineralogy and palaeomagnetic results

The demagnetization behaviour of NRM and SIRM is similar for all sites from Triassic, Permian and Carboniferous limestones as shown for a representative specimen in Fig. 4. IRM acquisition indicates pyrrhotite (≈ 90% saturation at about 500 mT) and additionally hematite or goethite (non-saturation up to 2.5 T). High coercivity behaviour during alternating field demagnetization, after removing possible goethite remanence by heating to 150 °C, also suggests pyrrhotite and hematite. Unblocking temperatures of 350–430 °C indicate a small amount of magnetite or maghemite (Fig. 4a,b). Thermal demagnetization of NRM and SIRM confirms pyrrhotite as the characteristic remanence carrier (ChRM with unblocking temperatures of 270–325 °C; Fig. 4a–c). Magnetic susceptibility monitored during heating shows magneto-mineralogical changes only above 450 °C. Predominantly, the remanence directions are of normal polarity, although, in some

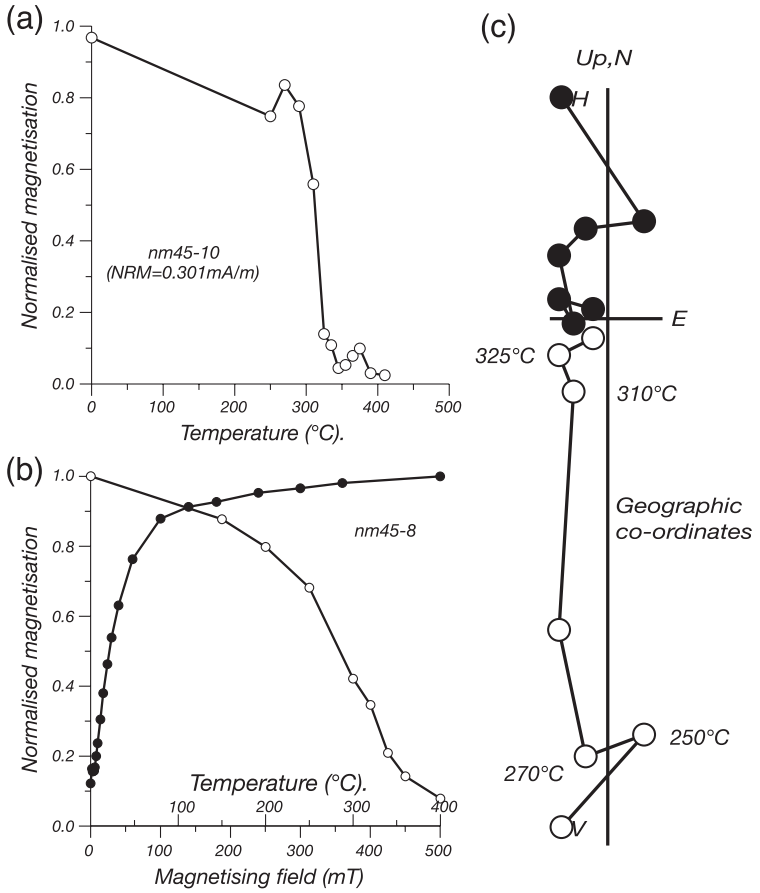

Fig. 4. Rock-magnetic and directional results of representative specimens from the low-grade metamorphic carbonates of the Nar/Phu valley. (a) Thermal demagnetization of NRM indicating pyrrhotite (unblocking spectrum of 270–325 °C). (b) IRM acquisition (full circles) and thermal demagnetization of SIRM (open circles) of specimen nm45-8. (c) Orthogonal vector projection of thermal demagnetization in geographic co-ordinates of specimen nm45-10.

samples a reverse or two antiparallel directions are observed. Linear principle component analysis was used for extraction of the ChRM. Statistical data of the ChRM are listed in Table 3. Well-grouped site mean directions and an overall mean direction in geographic co-ordinates of $D/I = 355.5/61.4$ ($\alpha_{95} = 16.5$, $k = 7.3$; Fig. 5; Table 3) are obtained (excluding site nc54, which reveals a random distribution of the ChRM directions). Site np43 seems to be an outlier, however, there is no reasonable argument to reject it. Influence of anisotropy on remanence directions or effects of local sliding are not obvious. Nevertheless, the overall mean direction excluding site np43 is similar ($D/I = 4.6/59.5$; $\alpha_{95} = 13.4$, $k = 11.4$). A negative fold test at 99% level of significance after McFadden (1990) indicates that the remanence acquisition occurred after the short-wavelength folding (F1 and F2). Partial unfolding of site mean directions shows a best grouping at −31% of unfolding. The high inclination excludes a recent origin of the ChRM (inclination of the present dipole field: $I_{present} = 47°$). Pyrrhotite is usually formed during low-grade metamorphism in marly carbonates at temperatures above 200 °C (Lambert, 1973; Carpenter, 1974). Remanence acquisition is likely of thermoremanent origin acquired during post-peak metamorphic cooling as indicated by the record of antiparallel components in single specimens, following interpretations of Crouzet et al. (2001). Therefore, the remanence age can be related to the cooling age through the Curie temperature of pyrrhotite ($T_c \approx 325$ °C). The origin of

Table 3
Statistical parameters for the pyrrhotite and magnetite component of the Nar/Phu valley (central Nepal)

Site	Latitude (°N)	Longitude (°E)	Altitude (m)	Dip Dir. (°)	Dip (°)	S	D_{geo} (°)	I_{geo} (°)	k	α_{95} (°)	D_{str} (°)	I_{str} (°)	k	α_{95} (°)
np43	28.782	84.273	4350	18–35	15–73	9	259.0	27.8	18.6	12.3	302.6	42.5	10.7	16.5
np44	28.786	84.273	4350	11–14	38–55	5	56.5	67.2	31.1	13.9	30.2	30.5	33.8	13.4
nm45	28.785	84.271	4400	10–26	40–45	8	289.3	78.5	81.2	6.2	4.8	45.6	76.7	6.4
nm46	28.786	84.271	4400	14–30	33–45	6	347.6	80.5	43.3	10.6	14.6	45.4	42.7	10.4
nm47	28.782	84.272	4430	190	86	9	328.1	55.5	39.4	8.3	215.5	28.5	39.4	8.3
nm48	28.782	84.272	4430	18	40	8	334.3	62.8	32.9	9.8	357.0	28.0	32.9	9.8
nm49	28.776	84.269	4530	208–222	67–80	6	5.9	53.9	50.5	9.5	241.4	48.3	46.1	10.0
nm50	28.776	84.269	4510	175–228	10–44	9	337.6	64.9	13.9	14.3	284.8	66.3	20.9	11.5
nm51	28.776	84.265	4530	238–285	15–23	9	4.2	45.1	25.0	10.5	346.3	44.6	26.4	10.2
nm52	28.776	84.264	4530	246–268	33–45	8	13.6	15.9	51.9	7.8	355.6	30.3	65.0	6.9
nm53	28.775	84.264	4530	260–290	24–54	10	32.8	63.1	30.8	8.8	329.5	60.5	16.8	12.1
nc54	28.767	84.276	4100	268–050	10–18	random distribution								
nc55	28.766	84.276	4120	260–302	15–29	8	201.7	−24.0	9.4	19.1	194.3	−23.4	8.4	20.3
nc56	28.769	84.275	4135	166–283	4–10	10	191.8	−65.8	29.4	9.1	186.2	−73.0	28.9	9.1
Pyrrhotite mean direction and statistics: $n = 13$ sites							355.5	61.4	7.3	16.5	354.4	47.3	4.7	21.4

N, E: geographic latitude, geographic longitude; S: number of specimens included in statistics; *D*, *I*: declination, inclination; geo, str: geographic/stratigraphic co-ordinates; α_{95}: 95% confidence angle; *k*: precision parameter; Dip Dir., Dip: dip direction and dip of bedding; *S*: number of specimens included for statistics; site codes (second index) m: Mukut Limestone, p: Permian Limestone, c: Carboniferous Limestone. All directions are interpreted as normal polarity except sites nc55 and nc56 (inverted for calculation of overall mean direction).

the ChRM post-dating the main deformation(s) F1 and F2 sets an upper limit to the age of remanence. As the deformation associated with F2 is responsible for peak temperature metamorphism (Godin, in press) and dated at ca. 35 Ma (Godin et al., 1999, 2001), the age of remanence acquisition is post-Eocene. K/Ar dating of illites, fission track dating of zircons and palaeothermometry constrain peak temperature conditions (330–370 °C) at 32–25 Ma for the Carboniferous to Triassic Tethyan formations in Manang area (Crouzet et al., 2002). As expected, peak temperature in these formations was only slightly higher than T_c of pyrrhotite (Crouzet et al., 2002), remanence has been likely acquired shortly after onset of cooling. The inclination is steeper by 28.6° to 20.4° (± 16.5°) than expected from the APWP (Acton, 1999) for an estimated age range of 32–25 Ma.

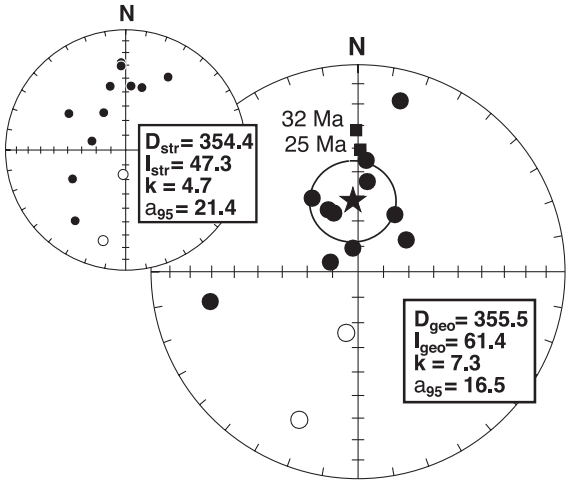

Fig. 5. Equal area projection of the site mean directions (open/full circles plotted in the upper/lower hemisphere) and the overall mean direction (star plotted in the lower hemisphere; reversed sites are inverted for calculation of overall mean direction). The full squares indicate the expected remanence direction calculated from the APWP (Acton, 1999, plotted in the lower hemisphere).

6. Discussion

The palaeomagnetic overall mean direction suggests a northward tilting of 20.4–28.6° since remanence acquisition at 25–32 Ma, respectively (Figs. 2b and 5). Oversteep inclinations were also observed in Manang area (Appel et al., 1991), the Everest leuco-granite (Rochette et al., 1994) and in Hidden valley (Crouzet et al., 2001) and have been interpreted as ramping on the Main Central Thrust (MCT).

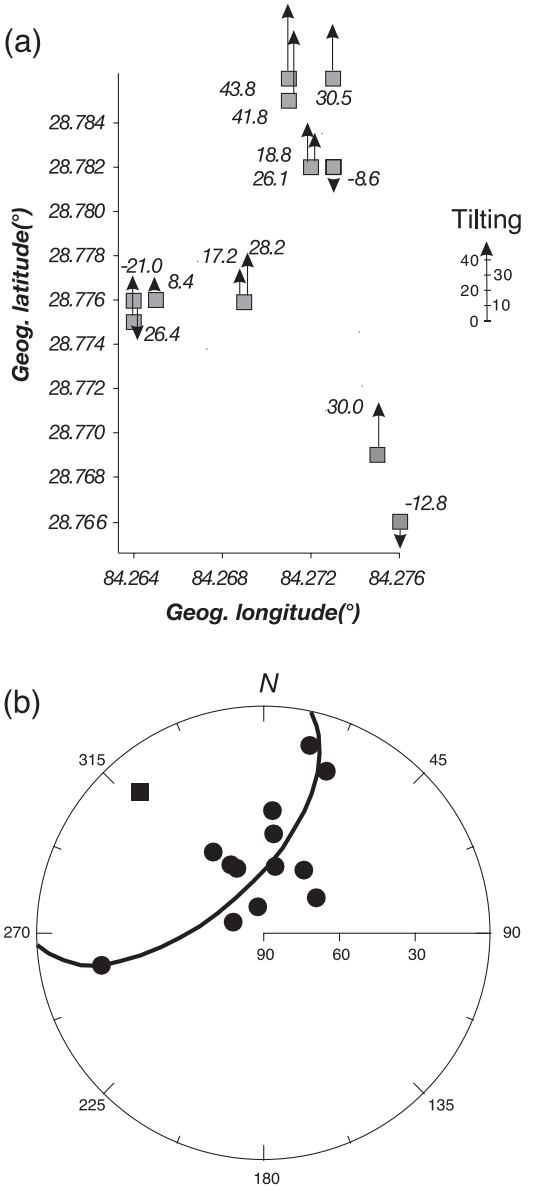

Fig. 6. (a) Spatial distribution of the tilting obtained for a mean magnetization age of 28.5 Ma. Angles of tilting are given and visualized by arrows (length proportional to the tilting angle; arrows to N/S denote northward/southward tilting, respectively). (b) Best-fitting small circle through the site mean directions of the secondary pyrrhotite component (circles). The pole of the small circle is shown by the square (confidence angle $\alpha_{95} = 3.2°$). Reversed sites (see Fig. 5) are inverted.

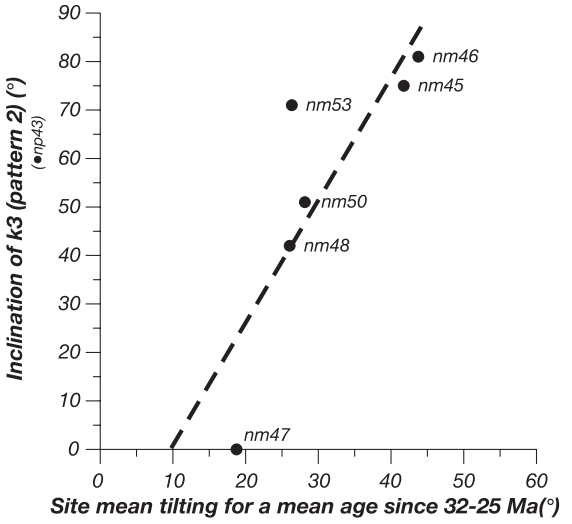

Fig. 7. Correlation between late-orogenic tilting (obtained from secondary pyrrhotite remanence directions) and the inclination of the site mean directions of the k3 axes of pattern P2 (np43 excluded).

Remanence acquisition at about 32 Ma is consistent with the Eohimalayan phase (constrained at 35–32 Ma by Guillot and Allemand, 2002), whereas the 25 Ma cannot be related to a major tectono-metamorphic phase. The mean inclination steepening coincides approximately with the 31° northward tilting caused by the formation of the Chako antiform in the study area. This indicates that the pyrrhotite remanence is older than the Chako antiform, which has a maximum age of 18 Ma (estimated according to the preliminary radiometric zircon U/Pb dating).

The tilting pattern on site level shows a variation with the geographic position (Fig. 6a), i.e. a trend of relatively higher tilting towards NE, reflecting a long-wavelength folding (several kilometers wavelength) associated to the Chako antiform. A corresponding fold axis can be modelled by least square fitting of a small-circle through the site mean directions (Fig. 6b) resulting in a pole at $D/I = 319°/19°$ ($\alpha_{95} = 3.2°$). Earlier observed steep inclinations have been interpreted in terms of MCT ramping (Appel et al., 1991; Rochette et al., 1994). However, the similarity between the steepening of remanence directions and the observed tilting by the Chakho antiform, as well as the steeper inclinations in the N of the sampling area suggest no influence of MCT ramping.

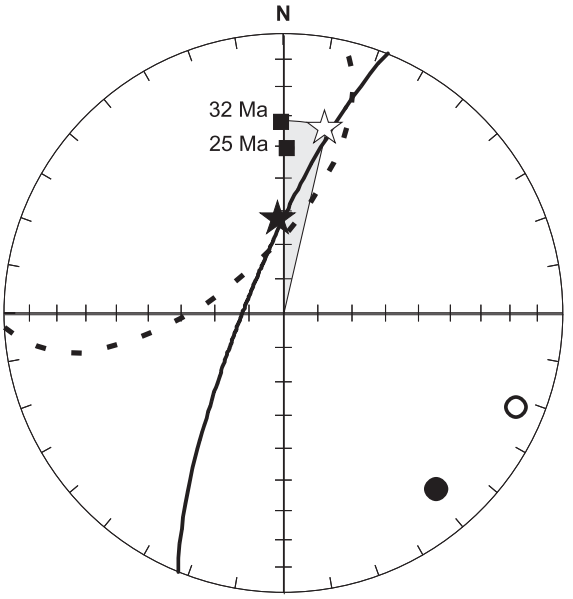

Fig. 8. Back-tilting of the observed remanence direction parallel to the remanence small circle in Fig. 6 (dashed line) and parallel to the great circle (full line) derived from AMS pattern P2, both indicating a clockwise rotation of about 16° (shown by the shaded area). Full star: measured overall remanence direction; open star: remanence direction obtained after back-tilting; squares: remanence directions expected from the APWP for 32 and 25 Ma. Full/open circle: mean fold axis derived from remanence/AMS data (plotted in the lower/upper hemisphere).

AMS patterns P1 and P2 seem to record different phases of the tectonic evolution. For P1, scattering of k1 axes (perpendicular to the fold axes) on site mean level becomes minimum when about 50% of 'unfolding' is applied by rotating k1 directions around the fold axis (intersection of bedding planes, coinciding with k3 of P1). This may be a hint for a syn-main folding origin of pattern P1 (short-wavelength folding F1 and F2). Pattern P2 shows rather well grouping of all axes indicating an origin during the latest stage of short-wavelength folding or even post-dating it. Correlation between late tectonic tilting of remanence directions (long-wavelength folding) and inclinations of k3 axes of P2 suggests that both represent in part the same deformation (Fig. 7). Assuming that the rotation axis of long-wavelength folding is horizontal (as it is indicated) relative tilting angles of remanence vectors and inclination of k3 axes of P2 should be equal. However, the slope of the regression line is clearly $\neq 1$ (Fig. 7). One explanation could be that P2 and P1 are not completely separated and inclinations of k3 axes are distorted systematically. Alternatively, only part of the long-wavelength folding might have been recorded by magnetic remanence whereas AMS may document it completely. Taking into account the U/Pb date, the latter case would imply that remanence acquisition is at least partly younger than 18 Ma.

Back-tilting of the overall ChRM to the direction expected from the APWP, parallel to the great circle defined by a pole corresponding to k1 of AMS P2 (or k3 of AMS P1 or the F2 fold axis), results in a clockwise rotation of 16° (Fig. 8). The same rotation angle is obtained (Fig. 8) by back-rotation parallel to the remanence small circle, using the small circle method of Waldhör et al. (2001). This method works with the small circle only and avoids the possible problem that the overall mean direction is determined from a non-Gaussian distribution of site means.

A compilation of the rotations obtained from neighbouring areas (Fig. 1 and Table 4) indicates an increasing clockwise rotation from the Hidden valley in the W to the Shiar valley in the E (a distance of

Table 4
Compilation of rotations obtained from secondary pyrrhotite remanences in central Nepal for the areas of Hidden valley (Crouzet et al., 2001), Thakkhola (B-component; Klootwijk and Bingham, 1980), Manang (Appel et al., 1991), Nar/Phu (this study), and Shiar valley (Schill et al., 2002)

	Hidden valley	Thakkhola	Manang	Nar/Phu	Shiar
Latitude	28.8°N,	28.7°N,	28.7°N,	28.8°N,	28.6°N,
Longitude	83.6°E	83.7°E	84.0°E	84.3°E	85.1°E
Age of remanence acquisition	30 ± 1 Ma	?	27.5 ± 2.5 Ma	32–25 Ma	25–17 Ma
Observed remanence direction	357.2/59.2 (3.6)	184.4/ − 54.3 (12.2)	196.4/ − 65.9 (3.2)	355.5/61.4 (not Fisher distributed)	206.9/ − 27.2 (not Fisher distributed)
Resulting mean cw rotation	− 2.3°	4.9°	16.6°	16°	26.5°

≈ 150 km). Oroclinal bending is unlikely to account for these clockwise rotations, because according to the model it should decrease to the E (Klootwijk et al., 1985).

7. Conclusions

Secondary pyrrhotite remanences are a potential tool for quantifying tectonic movements during late-orogenic deformation. Small circle analysis allows to separate a clockwise rotation (16°) and mean northward tilting (roughly 20–30°) related to long-wavelength folding in the studied area, which do not become obvious using a conventional palaeomagnetic interpretation scheme.

The occurrence of oversteep inclinations observed in the pyrrhotite component can be related to the formation of the Chako antiform (maximum age of ~ 18 Ma) rather than ramping directly along the MCT. However, a relation between a late motion along the MCT with break-back ramping and duplex structures as the cause of the Chako antiform is possible.

Long-wavelength folding is evidenced by the dispersion of remanence directions along a N–S profile. A small circle models this dispersion with a pole close to the F2 fold axis and close to the axis of the Chako antiform.

AMS patterns P1 and P2 reflect the main folding (short-wavelength folding F1 and F2) whereas the small circle distribution of the ChRM directions documents the formation of the Chako antiform (long-wavelength folding). Both reveal a similar fold axis.

According to tectono-metamorphic (peak temperature, geochronology, deformation history) and geophysical (fold test, T_c of pyrrhotite, occurrence of antiparallel components) constraints the possible age of remanence acquisition is 32–25 Ma postdating short-wavelength folding (F1 and F2) and predating the formation of the Chako antiform. However, correlation of k3 axes of AMS pattern P2 and remanence directions suggests that the deformation associated to the Chako antiform started before remanence acquisition was completed. If the proposed age of the Chako antiform is true (< 18 Ma), this would imply a younger age for the remanence (Early Miocene or younger. The general conclusions of a clockwise rotation and northward tilting would not be rejected by this complication, but the resulting angles would decrease.

Acknowledgements

We thank G. Fuchs for participation at the fieldwork and geological discussions. We like to thank the two reviewers D. Elmore and C. Aubourg for fruitful comments. This project was funded by the German Research Council (DFG). We acknowledge the financial support of the Natural Sciences and Engineering Research Council of Canada. This is ETH contribution No. 1294.

References

Acton, G.D., 1999. Apparent polar wander of India since the Cretaceous with implications for regional tectonics and true polar wander. Mem. Geol. Soc. India 44, 129–175.

Appel, E., Müller, R., Widder, R.W., 1991. Palaeomagnetic results from the Tibetan Sedimentary Series of the Manang area (north central Nepal). Geophys. J. Int. 104, 255–266.

Carpenter, R.H., 1974. Pyrrhotite isograde in the SE Tennessee and SW North Carolina. Geol. Soc. Amer. Bull. 85, 451–456.

Coleman, M., Hodges, K., 1998. Contrasting Oligocene and Miocene thermal histories from the hanging wall and footwall of south Tibetan detachment in the central Himalaya from 40Ar/39Ar thermochronology, Marsyandi Valley, Central Nepal. Tectonics 17 (5), 726–740.

Crouzet, C., Stang, H., Appel, E., Schill, E., Gautam, P., 2001. Detailed analysis of successive pTRMs carried by pyrrhotite in Himalayan metacarbonates: an example from Hidden Valley Central Nepal. Geophys. J. Int. 146, 607–618.

Crouzet, C., Paudel, L., Dunkl, I., Appel, E., Árkai, P., Balogh, K., Rainer, T.M., 2002. New constraints on the tectono-thermal evolution of the Tethyan Himalaya (Western Nepal). Abstracts for the 17th HKTW. J. Asian Earth Sci. 20 (4 Suppl. 1), 1–55.

DeCelles, P., Gehrels, G., Quade, J., Ojha, T.P., 1998. Eocene–early Miocene foreland development and the history of Himalayan thrusting, western and central Nepal. Tectonics 17 (5), 741–765.

Enkin, R.J., Osadetz, K.G., Baker, J., Kisilevsky, D., 2000. Orogenic remagnetizations in the front ranges and inner foothills of the southern Canadian Cordillera: chemical harbinger and thermal handmaiden of Cordilleran deformation. Geol. Soc. Amer. Bull. 112, 929–942.

Fuchs, G., Regmi, K., Schill, E., 1999. Note on the geology of the Nar–Manang region in northern Nepal (Himalaya). 14th Himalaya–Karakoram–Tibet International Workshop, Kloster Ettal. Terra Nostra 2, 46–47.

Garzanti, E., 1999. Stratigraphy and sedimentary history of the Nepal Tethys Himalaya passive margin. J. Asian Earth Sci. 17, 805–827.

Godin, L., 2001. The Chako dome: an enigmatic structure in the hanging wall of the South Tibetan detachment, Nar valley, central Nepal [abstract]. 16th Himalaya–Karakoram–Tibet Workshop Schloss Seggau, Austria. J. Asian Earth Sci. 19, 22–23.

Godin, L., 2003. Structural evolution of the Tethyan sedimentary sequence, central Nepal Himalaya. J. Asian Earth Sci. 21 (in press).

Godin, L., Brown, R., Hanmer, S., Parrish, R., 1999. Back folds in the core of the Himalayan orogen: an alternative interpretation. Geology 27 (2), 151–154.

Godin, L., Parrish, R., Brown, R.L, Hodges, K.V., 2001. Crustal thickening leading to exhumation of the Himalayan metamorphic core of central Nepal: insight from U–Pb geochronology and 40Ar/39Ar thermochronology. Tectonics 20, 729–747.

Guillot, S., Allemand, P., 2002. Two-dimensional thermal modelling of the early tectonometamorphic evolution in central Himalaya. J. Geodyn. 34 (1), 77–98.

Hodges, K.V., Parrish, R.R., Searle, M.P., 1996. Tectonic evolution of the central Annapurna range, Nepalese Himalayas. Tectonics 15, 1254–1291.

Jelinek, V., 1978. Statistical processing of anisotropy of magnetic susceptibility measured on group specimens. Stud. Geophys. Geod. 22, 50–62.

Klootwijk, C.T., Bingham, D.K., 1980. The extent of Greater India: III. Palaeomagnetic data from the Tibetan Series Thakkhola region, Nepal Himalaya. Earth Planet. Sci. Lett. 51, 381–405.

Klootwijk, C.T., Conaghan, P., Powell, C., 1985. The Himalayan Arc: large-scale continental subduction, oroclinal bending and back-arc spreading. Earth Planet. Sci. Lett. 75, 167–183.

Lambert, I.B., 1973. Post-depositional availability of sulphur and metals and formation of secondary textures and structures in stratiform sedimentary sulfide deposits. J. Geol. Soc. Aust. 20, 205–215.

Le Fort, P., Guillot, S., 1998. Preliminary results of Himlung expedition to northern Manaslu massif, central Nepal. In: Hamidullah, S., Lawrence, R.D., Qasim, J.M. (Eds.), 13th Himalaya–Karakoram–Tibet Int. Workshop. Geol. Bull., vol. 31. Univ. Peshawar, Pakistan, pp. 110–112.

McFadden, P.L., 1990. A new fold test for palaeomagnetic studies. Geophys. J. Int. 103, 163–169.

Rochette, P., Scaillet, B., Guillot, S., LeFort, P., Pecher, A., 1994. Magnetic properties of the High Himalayan leucogranites: structural implications. Earth Planet. Sci. Lett. 126, 214–234.

Schill, E., Appel, E., Zeh, O., Singh, V.K., Gautam, P., 2001. Coupling of late-orogenic tectonics and secondary pyrrhotite remanences: towards a separation of different rotation processes and quantification of rotational underthrusting in the western Himalayas (N-India). Tectonophysics 337, 1–21.

Schill, E., Appel, E., Gautam, P., Dietrich, P., 2002. Thermo-tectonic history of the Tethyan Himalayas deduced from palaeomagnetic record of metacarbonates from central Nepal (Shiar Khola). J. Asian Earth Sci. 20 (3), 203–210.

Schill, E., Crouzet, C., Gautam, P., Singh, V.K., Appel, E, in press. Where did rotational shortening occur in the Himalayas?–Inferences from palaeomagnetic analyses of remagnetisations. Earth Planet. Sci. Lett.

Searle, M.P., Godin, L., 2003. The South Tibetan detachment system and the Manaslu leucogranite: a structural reinterpretation and restoration of the Annapurna–Manaslu Himalaya Nepal. J. Geol. 111 (in press).

Thomas, J.C., Claudel, M.E., Collombet, M., Tricart, P., Dumont, T., 1999. First paleomagnetic data from the sedimentary cover of the French Penninic Alps: evidence for Tertiary counterclockwise rotations in the Western Alps. Earth Planet. Sci. Lett. 171, 561–574.

Vannay, J.C., Hodges, K.V., 1996. Tectonometamorphic evolution of the Himalayan metamorphic core between the Annapurna and Dhaulagiri, central Nepal. J. Metamorph. Geol. 14, 635–656.

Waldhör, M., Appel, E., Frisch, W., Patzelt, A., 2001. Palaeomagnetic investigation in the Pamirs and its tectonic implications. J. Asian Earth Sci. 19, 429–451.

Wyss, M., Hermann, J., Steck, A., 1999. Structural and metamorphic evolution of the northern Himachal Himalaya, NW India. Eclogae geol. Helv. 92, 3–44.